# Structured illumination fluorescence microscopy with distorted excitations using a filtered blind-SIM algorithm

R. Ayuk,[1] H. Giovannini,[1] A. Jost,[3,4] E. Mudry,[1] J. Girard,[1] T. Mangeat,[2] N. Sandeau,[1] R. Heintzmann,[3,4] K. Wicker,[3,4] K. Belkebir,[1] and A. Sentenac[1,*]

[1]*Aix-Marseille Université, Institut Fresnel, 13013 Marseille, France*

[2]*LBCMCP, CNRS Université Paul Sabatier Toulouse 3, 31062 Toulouse, France*

[3]*Institute of Photonic Technologies, Jena, Germany*

[4]*Institute of Physical Chemistry, Abbe Center of Photonics, Friedrich-Schiller-University Jena, Jena, Germany*

**Corresponding author: anne.sentenac@fresnel.fr*

Received May 30, 2013; revised September 12, 2013; accepted October 4, 2013; posted October 10, 2013 (Doc. ID 191448); published November 12, 2013

Structured illumination microscopy (SIM) is a powerful technique for obtaining super-resolved fluorescence maps of samples, but it is very sensitive to aberrations or misalignments affecting the excitation patterns. Here, we present a reconstruction algorithm that is able to process SIM data even if the illuminations are strongly distorted. The approach is an extension of the recent blind-SIM technique, which reconstructs simultaneously the sample and the excitation patterns without *a priori* information on the latter. Our algorithm was checked on synthetic and experimental data using distorted and nondistorted illuminations. The reconstructions were similar to that obtained by up-to-date SIM methods when the illuminations were periodic and remained artifact-free when the illuminations were strongly distorted. 

*OCIS codes:* (180.2520) Fluorescence microscopy; (100.6640) Superresolution; (100.3190) Inverse problems.
http://dx.doi.org/10.1364/OL.38.004723

In the last decade, numerous novel microscopy techniques that circumvent the Abbe limit and achieve super-resolution have emerged [1–5]. Among them, structured illumination microscopy (SIM) consists of recording several sample images for various positions and orientations of a periodic excitation pattern [6,7]. Because of the periodicity of the illumination, high spatial frequency information on the samples, which is usually filtered out in images obtained with uniform excitation, is down-modulated to lower frequencies and can be captured by a microscope. The information is extracted with simple algebra from a set of images obtained for different positions of the light grid and it is shifted back to its true position in Fourier space, thus extending the support region of the optical transfer function (OTF) of the microscope. The higher the frequency of the excitation patterns, the larger the OTF support and the better the resolution.

SIM has provided spectacular super-resolved images of biological samples in two and three dimensions [8,9], but it remains difficult to implement in practice. Indeed, for the correct extraction of the high frequency information, it is crucial that the excitation pattern remain periodic within the sample and that its position in each individual image be known with very high precision [8]. While spatial light modulators or mechanical means with active feedback control can ensure high precision and reproducibility of the pattern shape and position, less sophisticated systems may not be able to do so. Moreover, whatever the experimental control, the pattern distortion and misalignment induced by the sample itself cannot be avoided. This issue is particularly critical when super-resolution is sought with an illumination frequency close to the detection cutoff. It is thus highly desirable to develop SIM reconstruction algorithms that are able to cope with distorted patterns and unknown positions in order to extend the applicability domain of this promising microscopy technique.

To address misalignment issues, several procedures have been proposed to determine *a posteriori* the position and period of the excitation pattern from the raw images [10,11]. Yet, these techniques rely on the assumption that the pattern is periodic so they cannot handle distortion. Recently, a more general approach, named blind-SIM, has been proposed to process low-resolution sample images obtained with different unknown inhomogeneous (and possibly nonperiodic) excitation patterns [12]. The blind-SIM algorithm, which estimates iteratively both the sample and the illuminations, was shown to recover high-resolution fluorescence maps from low-resolution images obtained with random speckle illuminations. On the other hand, it remained less effective than standard SIM algorithms when the illuminations were periodic [12].

In this work, we adapt the blind-SIM approach in order to make it as efficient as an up-to-date SIM technique [10] when the illuminations are periodic (and whatever their periodicity), while robust to distortion and misalignments. First, we recall briefly the principles of blind-SIM that permit the reconstruction of a super-resolved map of the sample fluorescence density $\rho$ from $L$ low-resolution images $\{\zeta_l\}$ obtained with $L$ unknown inhomogeneous excitation patterns $\{I_l\}$.

The images are linked to the fluorescence density $\rho$ by the relation

$$\zeta_l = (I_l \rho) * p, \tag{1}$$

where $*$ stands for the convolution product and $p$ is the point spread function (PSF) of the optical device. For

 

the sake of simplicity, Eq. (1) is rewritten in a more condensed form using operator notation

$$\zeta_l = \mathbf{A}(I_l \rho). \tag{2}$$

To ameliorate the data-to-unknowns ratio, one introduces the reasonable constraint that the illuminations average is roughly homogenous over the sample [12],

$$\sum_{l=1}^{L} I_l \approx I_0, \tag{3}$$

where $I_0$ is a constant. In addition, *a priori* information stating that $\rho$ is positive is included in the inversion scheme. This is accomplished through the reconstruction of an auxiliary function $\xi$ such that $\rho = \xi^2$ [13–15].

The blind-SIM reconstruction algorithm consists of determining $\xi$ and $\{I_l\}$ so that Eq. (2) and the constraint in Eq. (3) are best satisfied. This is done via the iterative minimization of the cost functional, $\mathcal{F}(\xi, \{I_l\})$ of the form [12]

$$\mathcal{F}(\xi, \{I_l\}) = \sum_{l=1}^{L-1} \|h_l\|^2 + \|h_L\|^2 \tag{4}$$

with $h_l = \zeta_l^{\text{mes}} - \mathbf{A}\xi^2 I_l$ are residual errors computed from Eq. (2) and $h_L = I_0 - \sum_{l=1}^{L=1} I_l$. Note that the norm $\|\cdot\|$ and later the inner product $\langle \cdot, \cdot \rangle$ involve an integration over the image size.

For each iteration step $n$, both $\xi$ and $I_l$ are updated according to the recursive relations

$$\xi_n = \xi_{n-1} + \alpha_n d_{n;\xi} \quad \text{and} \quad I_{l,n} = I_{l,n-1} + \beta_{l,n} d_{l,n;I}, \tag{5}$$

where $d_{n;\xi}$ and $d_{l,n;I}$ are the Polak–Ribière conjugate gradient updating directions [13,14] for the density of fluorophores and illuminations, respectively. The weighting coefficients $\alpha$ and $\beta$ are determined at each iteration step by minimizing the cost function $\mathcal{F}$. Expressions of $d_{n;\xi}$ and $d_{l,n;I}$ are of the form

$$d_n = g_n + \gamma_n d_{n-1}, \quad \text{with} \quad \gamma_n = \frac{\langle g_n, g_{n-1} \rangle}{\|g_{n-1}^2\|^2}, \tag{6}$$

where $g_n$ is the gradient of $\mathcal{F}$ with respect to either $\xi$ or $I$ and

$$\begin{aligned} g_{n;\xi} &= -4 \sum_{l=1}^{L} \xi_{n-1} I_{l,n-1} \mathbf{A}^\dagger h_{l,n-1}, \\ g_{l,n;I} &= -2\xi_{n-1}^2 \mathbf{A}^\dagger (h_{l,n-1} - h_{L,n-1}) \end{aligned} \tag{7}$$

with $\mathbf{A}^\dagger$ being the adjoint operator of $\mathbf{A}$.

Blind-SIM was applied to images obtained with uncontrolled speckles and periodic illuminations. While it always provided reconstructed fluorescence maps with super-resolution, it proved less effective than up-to-date SIM algorithms in the periodic illumination configuration. Indeed, it was observed that the restoration of the sample high frequency information weakened as the illumination frequency became closer to the detection cutoff and totally disappeared when the latter was beyond the detection cutoff.

To render blind-SIM competitive in the specific case of SIM configuration, we propose to introduce an additional constraint in the inversion procedure. In SIM, the sample is successively illuminated by $L$ sinusoidal light patterns corresponding generally to the interference of two grating orders, which are translated and rotated. Even if the experimental setup is not well calibrated and controlled, the localization of the three peaks forming the Fourier transform $\tilde{I}_l$ of each illumination is approximately known. To take advantage of this information in the reconstruction algorithm, we introduced an auxiliary variable $\hat{I}_l$ such that

$$\tilde{I}_l = \tilde{\hat{I}}_l \tilde{f}_l. \tag{8}$$

The filter $\tilde{f}_l$ was chosen so that $\tilde{I}_l$ remained confined about the theoretical peaks. It was expressed as a symmetrical sum of Gaussians centered about the theoretical spatial frequencies of the pattern with a unit maximum and adjustable widths. The inversion procedure remains similar to that previously described except that the cost functional depends now on $\xi$ and $\{\hat{I}_l\}$. The gradient with respect to $\{\hat{I}_l\}$ is now of the form,

$$g_{l,n;\hat{I}} = -2\xi_{n-1}^2 \mathbf{A}^\dagger (h_{l,n-1} - h_{L,n-1}) * f_l. \tag{9}$$

This novel version of blind-SIM, hereafter named filtered blind-SIM, requires one to optimize the widths of the Gaussians forming the filter $f_l$. A large width amounts to removing the constraint, while a small width is likely to block the solution into a local minimum. After several trials, we found that a width equal to 20% of the approximate light grid frequency was a good compromise. The inversion procedure is stopped when the cost function reaches a plateau.

To assess the performances of filtered blind-SIM, we compared its reconstructions to that obtained by an up-to-date SIM algorithm [10] for both synthetic and experimental data. Note that, presently, filtered blind-SIM has been implemented for two-dimensional data, which restricts its use to in-focus thin samples.

We first simulated a microscopy experiment in which a two-dimensional sample, described by $\rho(r, \theta) \propto [1 + \cos(40\theta)]$ where $(r, \theta)$ are the polar coordinates of $\mathbf{r}$ in the sample plane, see Fig. 1(a), was imaged by a detection PSF $h(r, \theta) = (J_1(\text{NA}k_0 r)/k_0 r)^2 k_0^2/\pi$ where $J_1$ is the first-order Bessel function of the first kind and $k_0 = 2\pi/\lambda$ is the free-space wavenumber with $\lambda \approx 630$ nm and NA $= 1.49$. The sample was illuminated by a sinusoidal light pattern with a period of 230 nm under three successive orientations, $\theta = 0$, $2\pi/3$, $4\pi/3$, for each of which three shifts of one-third of the period were performed. The images were synthesized following Eq. (1) and corrupted with Poisson noise and an additional Gaussian noise corresponding to the electronic noise. In Fig. 1(b), we plot the fluorescence map reconstructed by the SIM algorithm. As expected, the sample radial modulation was retrieved with a good contrast for arc-periods down to 125 nm, i.e., half the Rayleigh criterion,

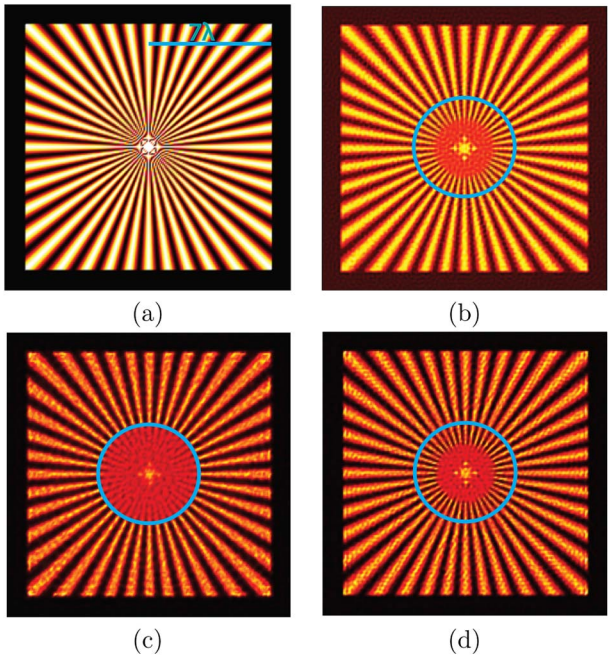


Fig. 1. Reconstructions of synthetic SIM images by several reconstruction methods. The blue circle delimitates the regions in which the arc-period of the radial modulation is above or below the Rayleigh criterion. (a) Fluorescence density of the radial sample, (b) reconstructed fluorescence map using the classical SIM algorithm [10], (c) reconstructed fluorescence map using a blind-SIM [12], and (d) reconstructed fluorescence map using a filtered blind-SIM.

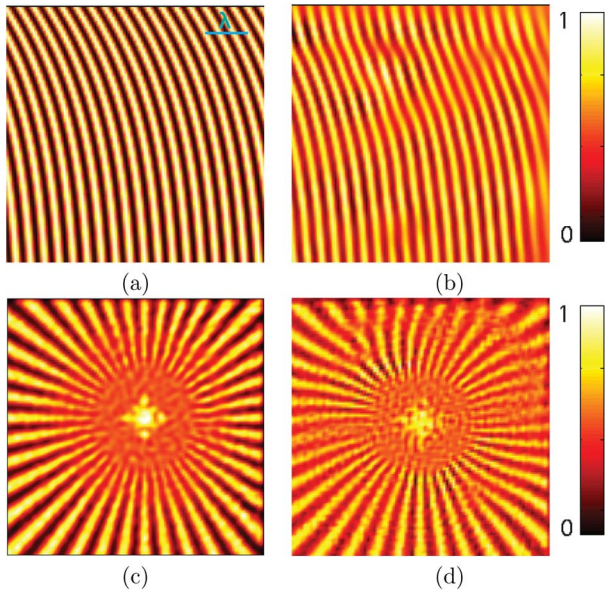


Fig. 2. Robustness of filtered blind-SIM and SIM algorithms with respect to pattern distortion. (a) One example of the distorted excitation pattern, (b) filtered blind-SIM estimation of the pattern displayed in (a), (c) filtered blind-SIM reconstruction of the sample, and (d) classical SIM reconstruction of the sample. The color scale indicates the normalized fluorophore density.

$0.6\lambda/\mathrm{NA} \approx 250$ nm. Meanwhile, the modulations reconstructed by blind-SIM beyond the Rayleigh criterion, while visible, exhibited poor contrast, see Fig. 1(c). On the other hand, the reconstruction provided by the filtered blind-SIM was similar to that given by SIM, and the modulation contrast remained close to one for arc-periods down to 125 nm similarly to SIM.

We then studied the robustness of the algorithms to pattern distortions. We considered illuminations that were deformed by optical aberrations (such as astigmatism and coma), as depicted in Fig. 2(a). We observed in Figs. 2(b) and 2(c) that the filtered blind-SIM was able to recover accurately the distorted illumination and provided an artifact-free super-resolved reconstruction. In contrast, the reconstruction obtained with the classical SIM algorithm shown in Fig. 2(d) was significantly deteriorated.

Finally, we analyzed the achievements of filtered blind-SIM on experimental data. A home-built SIM setup in the epi-illumination mode, similar to that described in [12], was used to record images of fluorescent samples excited by a sinusoidal light pattern with period of about 240 nm. The latter was formed on the sample through a high numerical aperture objective (NA = 1.49, 100X, CFI Plan Apochromat, Nikon) via the interference of the $\pm 1$ diffracted orders of a glass transmission grating (holographic, 80 lines/mm) placed in a secondary image plane of the microscope and illuminated with a collimated laser beam (He–Ne, 633 nm). Three orientations were obtained by rotating the grating successively by $2\pi/3$. For each orientation, the pattern was shifted eight times by translating horizontally the grating with a step of 30 nm (after magnification). The fluorescence light was separated from the laser reflection with a dichroic mirror and a fluorescence filter, and finally imaged on a camera (Andor iXon 897) with a pixel size of about 65 nm (after magnification). To study the robustness to patterns distortion, uncontrolled aberrations in the illumination wavefront were introduced by placing a transparent plastic sheet on the optical path of the illumination beams. The experiment was performed with and without distortion for the same image area and same imaging conditions. For all the reconstructions, the PSF was determined experimentally by averaging the images of isolated fluorophores present in the sample.

The sample consisted of fixed cancer cells in which the focal adhesion protein, paxillin, colocalized both in short fibrillary structures as well as tiny focal points was made fluorescent through interactions of a secondary rabbit monoclonal antibody marked with alexa 647 to a paxillin primary rabbit antibody.

Figures 3(a) and 3(b) display a small region of the reconstructed images obtained with filtered blind-SIM and SIM in the nondistorted case. One of the excitation patterns reflected by the sample coverslip and recorded on the camera without the fluorescence filter is shown in Fig. 3(c). From these results one can observe that filtered blind-SIM retrieves the same sample features as SIM though with a better resolution. The latter can be explained by the positivity constraint [16], which is particularly efficient on sparse samples. The artificially distorted case is examined in Figs. 3(d)–3(f). The excitation patterns passing through the plastic sheet were significantly deformed as shown in Fig. 3(f). Yet, the filtered blind-SIM image remains close to the one obtained in the

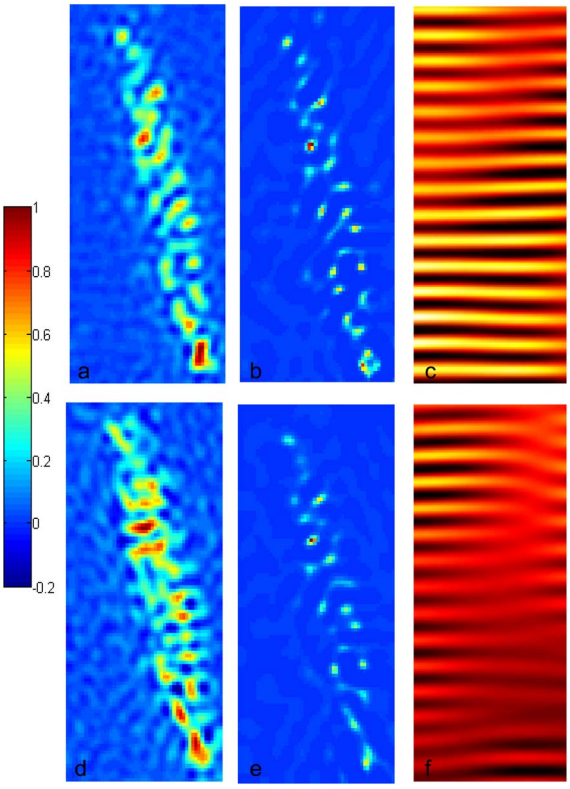


Fig. 3. Experimental results on fixed cells with marked paxillin for nondistorted [(a)–(c)] and artificially distorted [(d)–(f)] SIM configurations. The images size is 1.6 μm × 3.6 μm. (a) SIM image in the nondistorted case, (b) filtered blind-SIM image in the nondistorted case, (c) one example of the nondistorted illumination intensity, (d) SIM image obtained when the excitation patterns have been distorted by introducing a granular plastic sheet on the light path, (e) filtered blind-SIM in the distorted case, and (f) one example of the distorted illumination intensity.

nondistorted case, Figs. 3(b) and 3(d). In contrast, the SIM reconstruction was strongly degraded with both an increase in the background noise and important changes in the sample features, Figs. 3(a) and 3(c). Other experiments conducted with samples of fluorescent beads (not shown) yielded similar observations.

In conclusion, by reconstructing both the illuminations and the sample fluorescence, filtered blind-SIM was able to process SIM images even when the excitation patterns were strongly distorted. This technique proved as effective as up-to-date SIM algorithms when the illuminations were not distorted and significantly better when the illuminations were distorted. The method requires only an approximate knowledge of the pattern spatial frequencies (within 20% error margin) and does not necessitate any tuning of regularization parameters. Thus, it could permit a dramatic simplification of SIM implementation as the accurate control of the pattern is not necessary anymore. To extend its usefulness, filtered blind-SIM should now be adapted to three-dimensional data and thick samples. Work in this direction is in progress.

## References

1. T. A. Klar and S. W. Hell, Opt. Lett. **24**, 954 (1999).
2. M. Hofman, C. Eggeling, S. Jakobs, and S. W. Hell, Proc. Natl. Acad. Sci. USA **102**, 17565 (2005).
3. S. T. Hess, T. P. K. Girirajan, and M. D. Mason, Biophys. J. **91**, 4258 (2006).
4. E. Betzig, G. H. Patterson, P. Sougrat, W. Lindwasser, S. Olenych, J. S. Bonifacino, M. W. Davidson, and J. Lippincott-Schwartz, Science **313**, 1642 (2006).
5. M. J. Rust, M. Bates, and X. Zhuang, Nat. Methods **3**, 793 (2006).
6. R. Heintzmann and C. Cremer, Proc. SPIE **3568**, 185 (1999).
7. M. Gustafsson, J. Microsc. **198**, 82 (2000).
8. P. Kner, B. B. Chhun, E. R. Griffis, and L. W. M. G. Gustafsson, Nat. Methods **6**, 339 (2009).
9. L. Schermelleh, P. M. Carlton, S. Haase, L. Shao, L. Winoto, P. Kner, B. Burke, M. C. Cardoso, D. A. Agard, M. G. L. Gustafsson, H. Leonhardt, and J. W. Sedat, Science **320**, 1332 (2008).
10. K. Wicker, O. Mandula, G. Best, R. Fiolka, and R. Heintzmann, Opt. Express **21**, 2032 (2013).
11. S. A. Shroff, J. R. Fienup, and D. R. Williams, J. Opt. Soc. Am. A **26**, 413 (2009).
12. E. Mudry, K. Belkebir, J. Girard, J. Savatier, E. L. Moal, C. Nicoletti, M. Allain, and A. Sentenac, Nat. Photonics **6**, 312 (2012).
13. K. Belkebir and A. G. Tijhuis, Inverse Probl. **17**, 1671 (2001).
14. K. Belkebir and A. Sentenac, J. Opt. Soc. Am. A **20**, 1223 (2003).
15. A. Dubois, K. Belkebir, and M. Saillard, Inverse Probl. **21**, S65 (2005).
16. P. J. Sementilli, B. R. Hunt, and M. S. Nadar, J. Opt. Soc. Am. A **10**, 2265 (1993).